GEOLOGICA CARPATHICA, AUGUST 2018, 69, 4, 335–346 doi: 10.1515/geoca-2018-0020

Cummingtonite-bearing volcanic rocks: first evidence in the Central Slovak Volcanic Field

KATARÍNA ŠARINOVÁ[1, ✉] and SAMUEL RYBÁR[2]

[1]Department of Mineralogy and Petrology, Faculty of Natural Sciences, Comenius University in Bratislava, Mlynská dolina, Ilkovičova 6, 842 15 Bratislava, Slovakia; ✉sarinova@fns.uniba.sk
[2]Department of Geology and Paleontology, Faculty of Natural Sciences, Comenius University in Bratislava, Mlynská dolina, Ilkovičova 6, 842 15 Bratislava, Slovakia

(Manuscript received August 30, 2017; accepted in revised form May 31, 2018)

Abstract: Within the framework of reinterpretation of the depositional evolution of the Komjatice depression, presence of cummingtonite in weakly lithified sediment has been detected. The sediment is formed by volcanic lithoclasts and phenocrysts with a small admixture of non-volcanic grains. The different mineral composition and various degrees of alteration of volcanic lithoclasts, together with structural features point to epiclastic origin. Therefore, the studied samples can be described as volcanic paraconglomerate and sandstone. The cummingtonite is found in rusty coloured volcanic lithoclasts and in the heavy fraction. Cummingtonite-bearing volcanic rocks have not been described so far from the Slovak Neogene volcanic fields. Therefore its presence in the studied samples represents the first indication of such volcanic rock in Slovakia. The aim of the article is to invoke interest for finding these volcanic rocks in situ.

Keywords: cummingtonite, provenance, Komjatice depression, Danube Basin.

Introduction

The studied samples come from the Zlaté Moravce-1 well (ZM-1). The ZM-1 well is situated in the NE part of the Komjatice depression (Fig. 1; 48°22'25.75" N, 18°22'16.35" E) and was drilled in 1968–1969 during hydrocarbon prospection. Today, new petrographical and sedimentological research is taking place, with the aim of reinterpretation of the depositional history of the Danube Basin. On this occasion, Nafta Petroleum Company provided all the archive well cores for re-evaluation.

The Neogene marine sediments start at the depth of 1410–1405 m of ZM-1 well. They consist of mudstone, sandstone, volcanic conglomerate, volcanic-rich paraconglomerate to sandstone and bentonite layers (Šarinová et al. 2018). The objects of this study are sandy conglomerates to sandstones from the depth of 1005–1010 m and 1046–1051 m. These sediments were originally assigned to the late Badenian (early Serravallian) based on the Bul.-Bol. foraminiferal assemblages (Biela 1978). New biostratigraphic results assign the sediments from the depth of 1410–1046 m (core 12) to NN6 Zone (late Badenian–Sarmatian/Serravallian; Ozdínová 2012; Šarinová et al. 2018). But well core 11 from the depth of 1010–1005 m contains index Pannonian (Tortonian) fossils (Šarinová et al. 2018). Correlation of volcanic lithoclasts with their expected provenance is significant for this paper. Coarse-grained volcanic conglomerates from the depths 1346–1351 and 1099–1104 m are composed of sub-rounded pebbles to cobbles of biotite–amphibole andesites ± Px, Qz with tuffaceous matrix (Šarinová et al. 2018). The petrographic composition of conglomerates, together with the age range of surroundings sediments (NN6 Zone) allows the search for their provenance in the Studenec Fm. In the original works, the Studenec Fm. is formed by Bt–Amp andesite to dacite (SiO_2 57–68 %; Konečný et al. 1998a; Chernyshev et al. 2013). The Studenec Fm. forms the 3th evolutional stage of the Štiavnica stratovolcano (e.g., Konečný et al. 1998a, 2001; Konečný & Lexa 2001; Chernyshev et al. 2013). The presence of volcanic conglomerate and bentonite points to a dominance of the Štiavnica stratovolcano provenance at the time of sedimentation of the studied samples. High content of fresh amphibole in the analysed samples has led to explicit research connected with provenance analyses. In addition, fresh amphibole allowed for indirect K–Ar dating of sediments by dating volcanic activity. The aim of the paper is to bring information about the presence of cummingtonite-bearing volcanic lithoclasts in Neogene sediments. However, the main aim is to inspire volcanologists to discover their in situ occurrence among rocks of the Štiavnica stratovolcano.

Occurrence of cummingtonite and hornblende together in volcanic rocks has been described from a large number of felsic volcanic rocks and tephras. Cummingtonite with hornblende, orthopyroxene and biotite were described in rhyolites of the Okataina Volcanic Centre of New Zealand (Ewart & Green 1971; Ewart et al. 1975; Nicholls et al. 1992; Smith et al. 2005). Dacite Yn tephras of Mount St. Helens also contain cummingtonite with plagioclase, hornblende, magnetite and ilmenite in highly vesiculated microlite-free glass (Mullineaux 1986; Geschwind & Rutherford 1992). It was also described from andesites of the Narcondam volcano in the Andaman Sea

(Pal et al. 2007), from Iceland dacites at Króksfjördur volcano (Pedersen & Hald 1982), dacites from Martinique (d'Arco et al. 1981), Japan tephras (Matsu'ura et al. 2012) and other places. Moreover, the cummingtonite-bearing tephras are widely used in tephrostratigraphy (after Lowe & Hunt 2001), because they form only a low percentage of tephras and so can be used as correlation horizons (e.g., Matsu'ura et al. 2012). This fact can also be used for provenance studies, for example, of cummingtonite-bearing tephras connected with Mount St. Helens (Smith & Leeman 1982; Mullineaux 1986).

Methods

For the documentation of sedimentary structures well cores were cut in half, scanned and digitalized. Thin sections of well cores were analysed under polarization microscope. Two samples from the depth of 1046–1051 m and one sample from the depth of 1005–1010 m were used for heavy mineral analyses. Samples were washed in water and sieved to the fraction 0.25–0.10 mm. Heavy minerals were separated using heavy liquid and analysed under binocular microscope. Polished sections of heavy fraction and thin sections of studied sedimentary rock were analysed using WDS analysis of microprobe Cameca SX 100 (State Geological Institute of Dionýz Štúr), accelerating voltage 15 keV, probe current 20 nA. Raw analyses were recalculated to weight percent of oxide using ZAF correction. Inclusions of melt and mineral inclusion were determined by EDAX analyses. Only one melt inclusion was large enough for WDS analysis. Amphiboles were calculated after Hawthorne et al. (2012) using the Excel spreadsheet by Locock (2014). Pyroxene was calculated on the base of 6 anions, content of Fe^{3+} was calculated from stoichiometry after Dropp (1987). Plagioclase was calculated on the base of 8 anions. Groundmass in rusty coloured volcanic lithoclasts was also analysed. In this case, groundmass was replaced by secondary minerals. Their analyses were normalized to 44 total cation charges, to balance $O_{20}(OH)_4$ and all Fe was considered as Fe^{3+}. Groundmass analyses of these lithoclasts must be taken as informative, because the thin sections were not prepared and measured with respect to clay minerals. Whole rock chemical analysis of volcanic lithoclasts from Bt–Amp andesite (depth 1346–1351 m and 1099–1104 m) was done using ICP-ES (major oxides) and ICP-MS (trace elements) in Bureau Veritas mineral laboratories, Canada. Mineral abbreviations follow Whitney & Evans (2010).

Results

The studied core samples from the depth of 1046–1051 m (core 12) are typically rusty coloured and consist of two different lithological groups. The first is represented by poorly sorted, sandy paraconglomerate (Fig. 2b,d) with occasionally armoured mud intraclasts and indistinct synsedimentary folds. The clasts populate the full spectrum of roundness from poorly to well-rounded and reach up to 5 cm in diameter. Clasts are mostly of volcanic origin, and are highly varied in colour, in

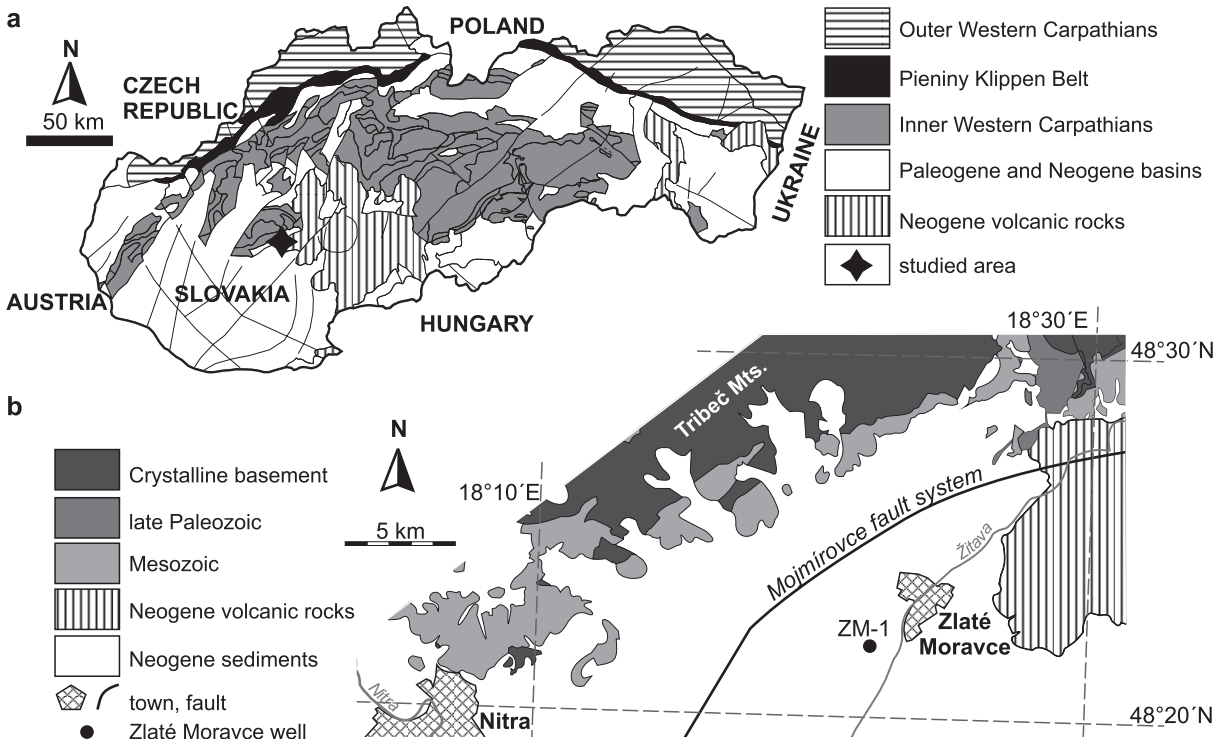

Fig. 1. a — Generalized geological map of Slovakia; **b** — schematic geological map showing the localization of the Zlaté Moravce-1 well (modified from the digital geological map of Slovakia, Káčer et al. 2013).

roundness and in the level of lithification. Some of these clasts are highly altered and have a tendency to weather out and so generate secondary porosity (Fig. 2b). The second group is represented by sandstones and mudstones with abundant erosional contacts, synsedimentary folds, faults and indistinct ripples (Fig. 2c). The core samples from the depth of 1005–1010 m (core 11) are very similar (Fig. 2a). But the content of non-volcanic clasts is higher and the sediment is occasionally better sorted. Matrix is less lithified.

In the depth 1046–1051 m, the gravel fraction (up to 2 mm) is composed of volcanic lithoclasts and phenocrysts of idiomorphic plagioclase. Non-volcanic admixture is present only in samples with observed muddy intraclasts. In the sandy fraction (2–0.06 mm) plagioclase phenocrysts together with volcanic lithoclasts strongly dominated, but quartz grains, heavy minerals, mudstone and sandstone lithoclasts are also present. Microscopic study of the thin sections documented idiomorphic to hypidiomorphic plagioclase, biotite, brown-green amphibole, pyroxene, poly- and monocrystalline quartz, opaque grains and lithoclasts. Lithoclasts are represented by volcanic rocks, but shale, sandstone and low grade Qz+Fs metasediments are also found together with foraminifera and mollusc shells. Planimetry was not done, but the amount of quartz grains and non-volcanic lithoclasts does not exceed ~10 %. Volcanic lithoclasts can be divided into two main types. The first type is represented by sub-rounded to rounded, lithified andesite clasts of greenish grey and light purple colour (Fig. 2b). Their porphyritic texture consists of phenocrysts of plagioclase and mafic minerals, which are often fully replaced by secondary minerals. However, large phenocrysts of brown, opacitized amphibole and biotite are observed (Fig. 3b), whereas quartz phenocrysts are rare. The first type of volcanic lithoclast groundmass is microcrystalline and is composed of K-feldspar, Pl and Qz. Rusty colouration is typical for the second type of volcanic lithoclast (Fig. 2b,d). The second type of lithoclast is porphyritic, rarely pilotaxitic and consists of phenocrysts of plagioclase, brown-green amphibole, biotite and pyroxene. Sometimes, pseudomorphs filled by secondary minerals are present. The presence of fresh pyroxene together with pyroxene shaped pseudomorphs in one

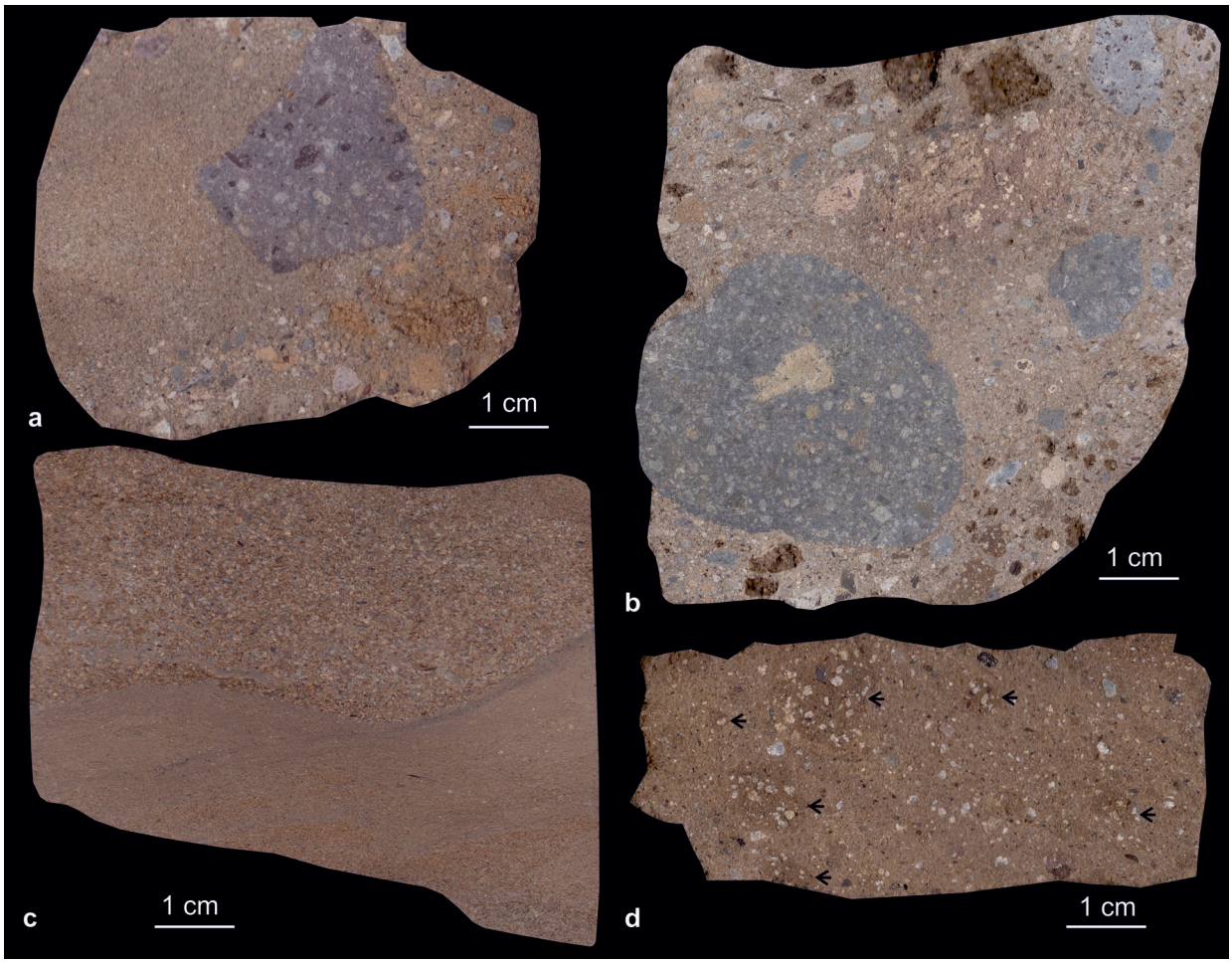

Fig. 2. Scanned well core samples: **a** —depth 1005 m, note the Bt–Amp andesite clast; **b** — depth 1046 m, note the rounded, andesite volcanic lithoclasts (first type) and rusty coloured, friable volcanic lithoclasts (second type); **c** — depth 1047 m, fossiliferous sandstones with indistinct ripples; **d** — depth 1051 m, the arrows point to rusty coloured volcanic clasts (second type).

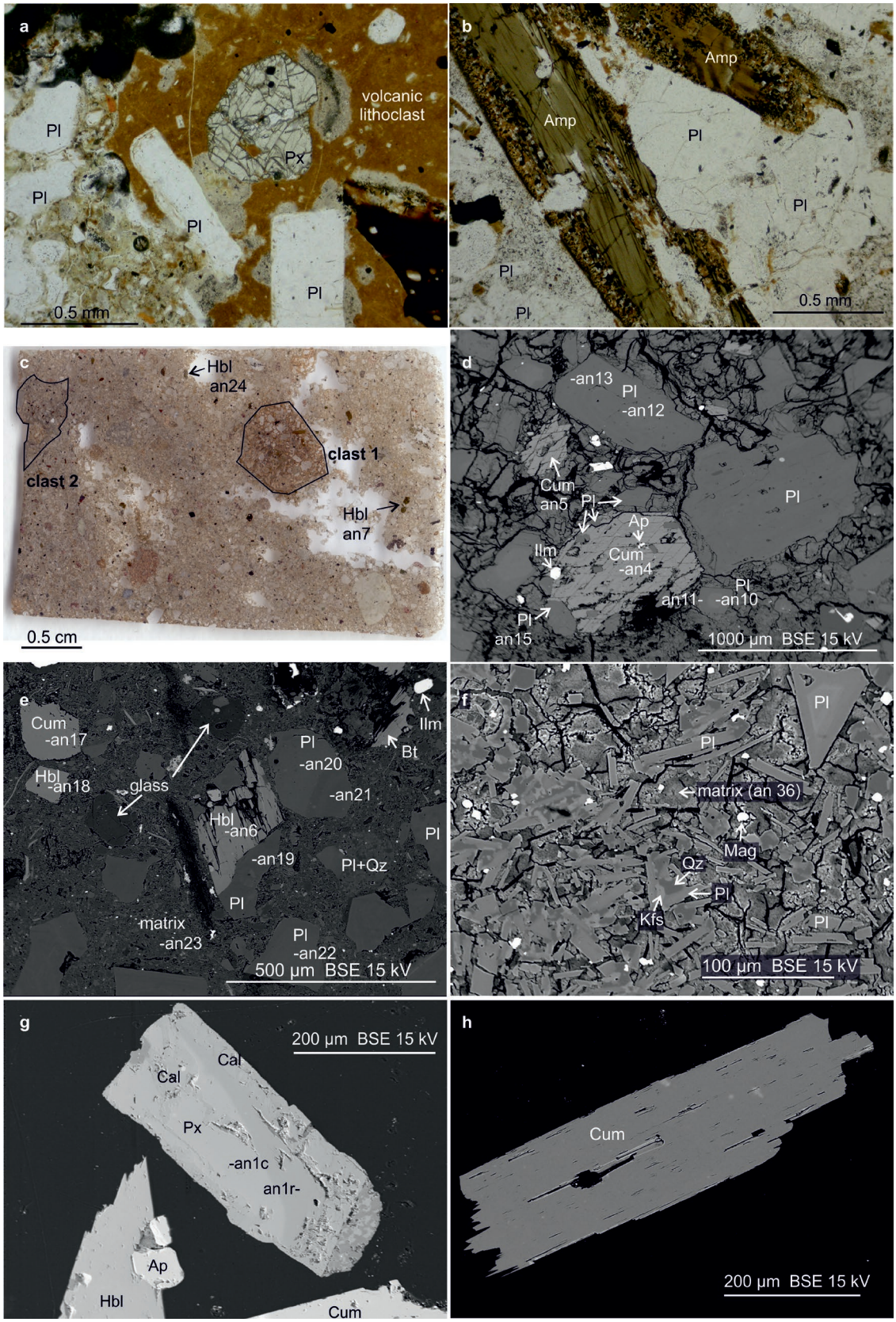

Fig. 3. a — Rusty coloured volcanic lithoclasts (second type; depth of 1046–1051 m), PPL; **b** — the first type of volcanic lithoclasts (depth 1046–1051 m), PPL; **c** — thin section of studied sediment with marked position of analysed cummingtonite-bearing lithoclasts (depth 1046–1051 m), scan; **d** — clast no. 1 (see **c**), BSE; **e** — clast no. 2 (see **c**), BSE; **f** — clast no. 3, BSE; **g** — zonal pyroxene from the heavy fraction, BSE; **h** — cummingtonite from the heavy fraction, BSE.

clast indicates two pyroxene types, where more stable clinopyroxene is preserved and orthopyroxene is decomposed. The second type is characterized by rusty coloured groundmass of lithoclasts that is composed of secondary minerals. However, part of these grains showed inhomogenity in the groundmass colouration (Fig.3a). Association is completed by clasts composed of vitroclasts and phenocrysts that are described as vitro-crystalloclastic tuffs. These results are confirmed by probe study of three rusty coloured volcanic lithoclasts of the second type. The studied clast number 1 (Fig. 3c,d.) with porphyritic texture and reddish colouration is composed of phenocrysts of cummingtonite (Table 1), plagioclase, biotite, apatite, titanomagnetite and ilmenite. Pl, Ilm, Ap and Ti-rich Mag are also present as mineral inclusions in cummingtonite phenocrysts (Fig. 3d). Plagioclase phenocrysts are zonal from An_{84} in the core to An_{50} in the rim (Table 2, Fig. 4). The indicative composition of the groundmass most closely corresponds to the Fe^{3+}-rich minerals of the smectite group (Table 1). Studied lithoclast number 2 (Fig. 3c,e) consists of vitroclasts, lithoclasts, plagioclase phenocrysts ($An_{73–50}$; Table 2, Fig. 4), magnesio-ferri-hornblende, cummingtonite (Table 1, Fig. 5), biotite and ilmenite. The combination of phenocrysts, vitroclasts and lithoclasts in Si-rich microlitic matrix enable us to classify the studied clast as a tuff. The analysed porphyritic, rusty coloured volcanic clast number 3 is composed of phenocrysts of zonal plagioclase ($An_{90–60}$; Table 2, Fig. 4) and phenocrysts of mafic minerals, that are fully replaced. The chemical composition of its groundmass is the same as in the clast 1 (Table 1), but some parts are not altered (Fig. 3f). They are formed by microcrystals of quartz, K-feldspar and

Table 1: The composition of amphiboles from volcanic lithoclasts and mineral grains, together with an indicative composition of groundmass from volcanic lithoclasts (the thin section was not prepared with respect to clay mineral analysis); ***** values were calculated according to Locock (2014), X_{Fe}=Fe/(Fe+Mg+Mn+Ca).

Species	**magnesio-ferri-hornblende**				**cummingtonite**							**groundmass**		
Clast no.	**Clast 2**		**mineral grain**		**Clast 1**					**Clast 2**		**Clast 1**	**Clast 2**	**Clast 3**
Anal.	**6**	**17**	**7**	**24**	**1**	**2**	**3**	**4**	**5**	**18**		**16**	**23**	**36**
SiO_2	46.81	47.12	46.94	46.10	53.01	53.61	52.41	53.31	52.53	53.34	SiO_2	50.63	87.02	49.44
TiO_2	1.00	1.15	1.31	1.14	0.33	0.23	0.36	0.26	0.34	0.27	TiO_2	0.15	0.09	0.12
Al_2O_3	7.92	7.92	8.13	8.30	2.21	1.92	2.90	2.16	2.58	2.04	Al_2O_3	8.60	6.40	8.60
Cr_2O_3	0.03	0.01	0.00	0.00	0.00	0.00	0.00	0.01	0.00	0.03	Cr_2O_3	0.02	0.04	0.02
MnO	0.40	0.33	0.31	0.50	0.70	0.73	0.78	0.79	0.77	0.81	MnO	0.24	0.02	0.24
FeO	16.85	15.45	16.32	17.32	22.44	23.18	23.63	22.38	22.53	21.74	FeO	17.04	1.66	15.85
NiO	0.00	0.02	0.00	0.03	0.01	0.00	0.00	0.00	0.00	0.01	NiO	0.00	0.01	0.01
MgO	12.23	12.76	12.18	11.73	16.89	16.77	15.89	16.88	16.18	17.23	MgO	12.66	1.26	11.52
CaO	10.02	10.42	10.62	10.28	1.48	1.02	1.24	1.66	1.85	1.58	CaO	2.31	0.38	2.65
Na_2O	1.20	1.31	1.33	1.35	0.33	0.29	0.44	0.30	0.41	0.33	Na_2O	0.31	0.46	0.22
K_2O	0.36	0.42	0.53	0.42	0.01	0.00	0.01	0.00	0.01	0.00	K_2O	0.33	1.37	0.32
F	0.00	0.00	0.00	0.00	0.00	0.00	0.00	0.00	0.00	0.00	F	0.00	0.00	0.00
Cl	0.13	0.12	0.16	0.14	0.05	0.04	0.03	0.04	0.04	0.03	Cl	0.06	0.02	0.12
Init. tot	96.91	96.99	97.78	97.27	97.44	97.79	97.67	97.78	97.24	97.40	*Total*	92.35	98.72	89.09
*FeO	12.81	11.40	12.55	12.59	21.85	23.00	22.87	21.89	21.81	21.24	Si	7.279		7.341
*Fe_2O_3	4.49	4.50	4.19	5.26	0.65	0.21	0.84	0.55	0.80	0.56	Al	0.721		0.659
*H_2O^+	2.01	2.02	2.00	2.00	2.05	2.04	2.04	2.05	2.04	2.06	*T subtot*	8.000		8.000
Tot.	99.37	99.46	100.20	99.80	99.56	99.85	99.80	99.88	99.36	99.52	Al	0.736		0.846
Si	6.918	6.920	6.882	6.815	7.760	7.833	7.694	7.777	7.724	7.789	Ti	0.016		0.013
Al	1.082	1.080	1.118	1.185	0.240	0.167	0.306	0.223	0.276	0.211	Fe^{3+}	1.366		1.312
Ti	0.000	0.000	0.000	0.000	0.000	0.000	0.000	0.000	0.000	0.000	Mg	2.713		2.550
Fe^{3+}	0.000	0.000	0.000	0.000	0.000	0.000	0.000	0.000	0.000	0.000	Mn	0.029		0.030
T subtot	8.000	8.000	8.000	8.000	8.000	8.000	8.000	8.000	8.000	8.000	Cr	0.002		0.002
Ti	0.111	0.127	0.144	0.127	0.036	0.025	0.039	0.029	0.037	0.029	Ni	0.000		0.001
Al	0.297	0.291	0.287	0.262	0.140	0.163	0.197	0.148	0.170	0.139	*M subtot*	4.863		4.753
Cr	0.004	0.001	0.000	0.000	0.000	0.001	0.000	0.001	0.000	0.004	Ca	0.355		0.421
Fe^{3+}	0.501	0.497	0.462	0.585	0.072	0.022	0.094	0.060	0.089	0.062	K	0.061		0.061
Ni	0.000	0.002	0.000	0.003	0.002	0.000	0.000	0.000	0.000	0.001	Na	0.088		0.064
Fe^{2+}	1.394	1.288	1.445	1.437	1.063	1.136	1.194	1.091	1.157	1.013	*I subtot*	0.504		0.546
Mg	2.693	2.794	2.662	2.585	3.686	3.653	3.477	3.670	3.547	3.752				
C subtot	5.000	5.000	5.000	4.999	4.999	5.000	5.001	4.999	5.000	5.000				
Mn^{2+}	0.050	0.041	0.039	0.062	0.087	0.090	0.096	0.097	0.096	0.100				
Fe^{2+}	0.188	0.113	0.095	0.119	1.611	1.674	1.614	1.579	1.524	1.580				
Ca	1.586	1.639	1.669	1.628	0.232	0.159	0.195	0.260	0.291	0.247				
Na	0.176	0.207	0.198	0.190	0.070	0.076	0.095	0.064	0.089	0.072				
B subtot	2.000	2.000	2.001	1.999	2.000	1.999	2.000	2.000	2.000	1.999				
Na	0.167	0.166	0.179	0.195	0.024	0.007	0.031	0.020	0.029	0.020				
K	0.067	0.079	0.099	0.079	0.002	0.000	0.001	0.000	0.003	0.000				
A subtot	0.234	0.245	0.278	0.274	0.026	0.007	0.032	0.020	0.032	0.020				
O	22.000	22.000	22.000	22.000	22.000	22.000	22.000	22.000	22.000	22.000				
OH	1.967	1.971	1.960	1.965	1.989	1.990	1.992	1.989	1.990	1.992				
F	0.000	0.000	0.000	0.000	0.000	0.000	0.000	0.000	0.000	0.000				
Cl	0.033	0.029	0.040	0.035	0.011	0.010	0.008	0.011	0.010	0.008				
W subtot	2.000	2.000	2.000	2.000	2.000	2.000	2.000	2.000	2.000	2.000				
Cat Sum	15.234	15.245	15.279	15.272	15.025	15.006	15.033	15.019	15.032	15.019				
X_{Fe}					0.407	0.421	0.435	0.404	0.413	0.393				

Table 2: The composition of feldspar from volcanic lithoclasts and mineral grains; c — core, r — rim, phen — phenocrysts, matrix — microcrystals from groundmass of clasts (see Fig. 3f).

Location	Clast 1					Clast 2				Clast 3				Mineral grain	
Anal.	10 Phen. 2c	11 Phen. 2r	12 Phen. 3c	13 Phen. 3r	15 Phen. 5	19 Phen. 6	20 Phen. 7c	21 Phen. 7r	22 Phen. 8	30 Phen. 12c	31 Phen. 12r	33 matrix 14	35 matrix 15	25 Phen. 9c	26 Phen. 9r
SiO_2	46.62	54.45	51.04	55.82	54.51	51.80	49.51	55.10	49.54	45.18	53.28	65.22	57.85	46.47	53.48
Al_2O_3	33.21	28.18	30.76	27.32	28.24	30.08	31.78	27.67	31.11	34.78	29.47	20.40	27.53	33.70	28.83
SrO	0.10	0.09	0.10	0.11	0.07	0.05	0.07	0.12	0.07	0.08	0.07			0.08	0.07
FeO	0.50	0.42	0.22	0.35	0.65	0.48	0.29	0.21	0.27	0.24	0.29	0.30	0.64	0.29	0.32
MgO	0.00	0.00	0.00	0.00	0.00	0.00	0.01	0.00	0.00	0.00	0.00	0.00	0.04	0.01	0.00
BaO												0.80	0.06		
CaO	17.24	11.10	13.99	10.30	11.02	13.35	14.97	10.59	14.61	18.50	12.35	0.56	8.34	17.55	12.11
Na_2O	1.75	4.83	3.77	5.60	5.17	3.85	3.00	5.48	3.23	1.11	4.62	4.32	6.07	1.56	4.41
K_2O	0.06	0.94	0.15	0.39	0.23	0.20	0.11	0.31	0.12	0.04	0.21	9.99	0.97	0.05	0.51
Tot.	*99.46*	*100.02*	*100.05*	*99.89*	*99.89*	*99.81*	*99.74*	*99.48*	*98.96*	*99.93*	*100.28*	*101.59*	*101.52*	*99.69*	*99.73*
Si	2.161	2.471	2.327	2.523	2.471	2.363	2.270	2.501	2.288	2.089	2.411	2.927	2.565	2.147	2.434
Al	1.814	1.507	1.653	1.455	1.509	1.617	1.717	1.481	1.693	1.895	1.572	1.079	1.439	1.835	1.546
Ti	0.003	0.002	0.003	0.003	0.002	0.001	0.002	0.003	0.002	0.002	0.002	0.000	0.000	0.002	0.002
Fe	0.019	0.016	0.009	0.013	0.025	0.018	0.011	0.008	0.011	0.009	0.011	0.011	0.024	0.011	0.012
Mg	0.000	0.000	0.000	0.000	0.000	0.000	0.000	0.000	0.000	0.000	0.000	0.000	0.003	0.000	0.000
Ba	0.000	0.000	0.000	0.000	0.000	0.000	0.000	0.000	0.000	0.000	0.000	0.014	0.001	0.000	0.000
Ca	0.856	0.540	0.684	0.499	0.535	0.652	0.735	0.515	0.723	0.917	0.599	0.027	0.396	0.869	0.590
Na	0.157	0.425	0.333	0.490	0.455	0.341	0.267	0.483	0.289	0.099	0.405	0.376	0.522	0.140	0.389
K	0.003	0.055	0.009	0.023	0.013	0.012	0.006	0.018	0.007	0.002	0.012	0.572	0.055	0.003	0.030
Cat sum	5.013	5.016	5.017	5.006	5.009	5.005	5.008	5.008	5.013	5.014	5.012	5.007	5.004	5.007	5.003
Or %	0.32	5.35	0.87	2.23	1.33	1.15	0.61	1.74	0.67	0.25	1.20	58.69	5.65	0.29	2.95
Ab %	15.46	41.71	32.50	48.47	45.32	33.91	26.46	47.54	28.37	9.75	39.87	38.53	53.65	13.82	38.58
An %	84.22	52.94	66.63	49.31	53.35	64.94	72.93	50.72	70.96	90.00	58.93	2.78	40.70	85.89	58.47

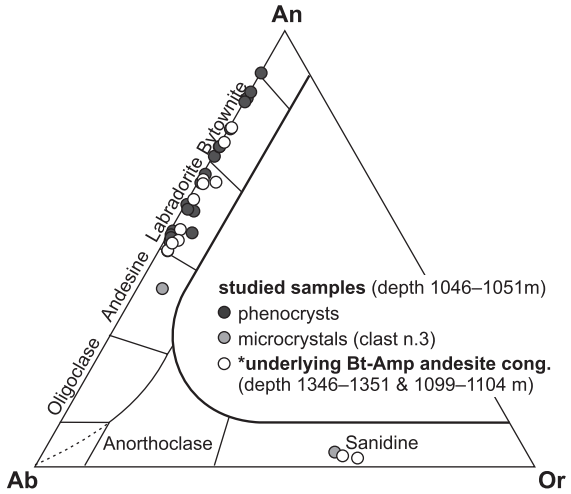

Fig. 4. Diagram of feldspar composition; *analyses taken from Šarinová et al. (2018).

plagioclase (An_{40}). With the exception of volcanic lithoclasts, some mineral grains of plagioclase ($An_{85–51}$) and amphibole (Hbl) are also analysed (Tables 1, 2).

Samples from the depth 1005–1010 m show a very similar composition (Fig. 2a). However, the content of non-volcanic lithoclasts is higher (~25 % in fraction up to 2 mm). Non-volcanic lithoclasts are composed of quartz arenite, sandstone, metasandstone, quartzite, chert, granitoid and polycrystalline quartz. All previously described volcanic lithoclast types are also present. Mineral grains are formed by quartz, amphibole, biotite and plagioclase.

The heavy fractions from the depth of 1046–1051 m contain mainly amphibole grains (50 %). Ilmenite together with magnetite forms 36–44 %, pyrite, framboidal pyrite and limonitized pyrite 2.5–6.9 %, apatite 2.5–2.8 %, and pyroxene 1.6 %. The association is supplemented with zircon, tourmaline, rutile, titanite and garnet (less than 1 %). In the heavy fraction from the depth of 1010–1005 m amphibole dominates (79 %). Ilmenite together with magnetite forms 16 %, pyrite, framboidal pyrite and limonitized pyrite form 2.7 %. The amount of apatite, pyroxene, zircon, tourmaline, rutile, titanite and garnet is less than 1 %. Such heavy mineral associations are typical for a volcanic source area. Zircon and tourmaline represented non-volcanic admixture, whereas framboidal pyrite is an authigenic mineral, which indicates a marine environment. During the study of heavy mineral association under the binocular microscope two types of amphiboles with different colour were distinguished. Black coloured amphiboles (Hbl) dominated, whereas less coloured and more transparent amphiboles (Cum) are less frequent.

The composition of amphiboles from the heavy fraction is consistent with previous results (Table 3, Fig. 5). From the Ca-amphibole subgroup, magnesio-ferri-horblende and minor magnesio-hastingsite are present. Inside the hornblende grains, inclusions of melts, plagioclase, titanomagnetite and apatite are observed. Melt inclusions show a rhyolite composition (Table 3). The Mg–Fe–Mn amphibole subgroup is represented by cummingtonite. In cummingtonite grains no mineral or melt inclusions have been observed (Fig. 3f). Both amphibole subgroups are without zonality (Fig. 3h), but the zonality of augite is determined (Fig. 3g). From core to rim the Mg content slightly increases and the Fe content decreases (Table 4). Marginal parts of augite are replaced by carbonate (Fig. 3g).

For interpretation of amphibole provenance, the composition of amphiboles from underlying volcanic conglomerates (depths 1346–1351 m and 1099–1104 m) is also analysed. These rocks mainly contain magnesio-hastingsite with weak zoning, but some phenocrysts have magnesio-ferri-hornblende composition (Table 5, Fig. 5a). Whole rock chemical analyses of lithoclasts were made to confirm the provenance of the Bt–Amp andesite conglomerates in the Studenec Fm. (Table 6). Results of analyses display andesitic composition, which is similar to Bt–Amp andesite to dacite of the Studenec Fm. (Fig. 6).

Discusion

The association of cummingtonite, hornblende, hastingsite and pyroxene was first observed in the heavy fraction. Rare presence of hastingsite in heavy fraction can be explained by reworking of underlying Bt–Amp andesite conglomerates (depth 1346–1351 m and 1099–1104 m; Table 5, Fig. 5), or by their ongoing erosion in the source area. In the Bt–Amp andesite hastingsite is present. Observed phenocrysts of brown amphibole in the first type of studied lithoclasts clearly confirmed this provenance (Fig. 3b). In the Bt–Amp andesite conglomerate, hastingsite phenocrysts are dominant and hornblende is less frequent (Fig. 5a). But, in the studied samples the opposite situation is observed. The large portion of hornblende with regard to hastingsite in the studied samples, excludes the provenance of hornblende strictly from underlying Bt-Amp andesite conglomerates. In addition, these conglomerates do not contain cummingtonite. For this reason, the source of hornblende and cummingtonite must be found in other volcanic rocks. This result is supported by the presence of large, relatively fresh phenocrysts of pyroxene. In the underlying Bt–Amp andesite conglomerate pyroxene is rare and fully altered.

In the volcanic fields of Slovakia, cummingtonite-bearing volcanic rocks have never been recorded. Cummingtonite was described only from the KON-1 well (Javorie Mts.) as a product of interaction between magma and Ca-silicate xenoliths (Hraško et al. 2014) and from the reaction rim of pargasite in rhyolites of the Strelníky Fm. (Kollárová 2010). These rare occurrences of microcrystalline cummingtonite associated with alterations and decay of primary minerals cannot explain the presence of cummingtonite in the 0.25–0.10 mm fraction. Cummingtonite was also described in metabasic rocks (e.g., Faryad & Zábranský 1996; Janák et al. 2001). However, there are no indications of metabasic rocks in the petrographic composition of the studied samples and surrounding sediments (Šarinová et al. 2018). On the other hand, detailed probe study of selected volcanic lithoclasts of the second type (rusty colour) clearly demonstrated volcanic origin of the cummingtonite phenocrysts (Fig. 3d). The calculated X_{Fe} (Fe/(Fe+Mn+Mg+Ca) of cummingtonite is 0.43–0.39, which is consistent with published data from cummingtonite phenocrysts of volcanic origin (0.42–0.33; e.g., Evans & Ghiorso 1995; Smith et al. 2005). The mineral association in the studied sediments (plagioclase, pyroxene, hornblende, cummingtonite, biotite and monocrystalline quartz) is also consistent with the occurrence of cummingtonite-bearing volcanic rocks in the world (Ewart & Green 1971; Ewart et al. 1975; Mullineaux 1986; Nicholls et al. 1992; Geschwind & Rutherford 1992; Smith et al. 2005; Pal et al. 2007; Fig. 7). However, the co-occurrence of cummingtonite and hornblende is documented only in tuff-type lithoclast (Fig. 3e). The composition of marginal parts of plagioclase phenocrysts ($An_{53–49}$) and microcrystalline matrix (An_{40}) in volcanic lithoclasts (second type) is typical for andesitic or dacitic volcanic rocks. The content of An molecule and zonality of plagioclase phenocrysts are very similar to Pl phenocrysts in the underlying

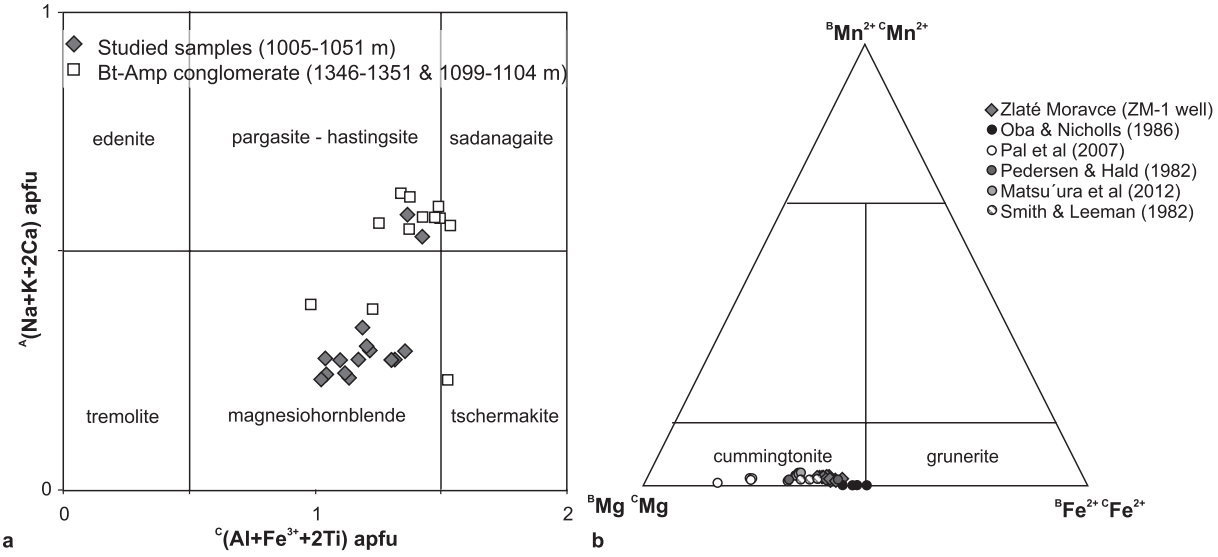

Fig. 5. Amphibole classification diagrams (Hawthorne et al. 2012) shows amphiboles from studied samples and from underlying Bt–Amp andesite conglomerate: **a** — the Ca amphibole subgroup; **b** — Mg–Fe–Mn amphibole subgroup. Note the composition of cummingtonite from literature (Pedersen & Hald 1982; Smith & Leeman 1982; Oba & Micholls 1986; Pal et al. 2007; Matsu'ura et al. 2012 — average data).

Table 3: The composition of selected amphiboles from heavy fraction; ***** values were calculated according to Locock (2014), X_{Fe}=Fe/(Fe+Mg+Mn+Ca)

Species	**magnesio-ferri-hornblende**						**magnesio-hastingsite**		**cummingtonite**						**melt**
Anal.	**2**	**9**	**10**	**11**	**12**	**15**	**6**	**17**	**13**	**14**	**19**	**20**	**21**	**22**	**inclusion**
SiO_2	46.22	44.95	45.07	46.25	45.43	46.38	42.73	42.91	52.35	52.56	53.30	52.59	53.53	53.02	73.75
TiO_2	0.86	1.13	1.85	1.22	1.38	1.03	1.75	1.66	0.33	0.26	0.21	0.34	0.21	0.25	0.10
Al_2O_3	8.34	9.23	9.18	8.57	9.01	7.87	12.86	13.88	2.40	2.12	1.58	2.39	1.84	1.74	11.92
Cr_2O_3	0.01	0.01	0.01	0.01	0.04	0.00	0.12	0.00	0.00	0.00	0.00	0.00	0.00	0.02	0.00
MnO	0.55	0.48	0.35	0.44	0.48	0.45	0.11	0.20	0.92	0.97	0.81	0.89	0.98	0.92	0.08
FeO	17.54	17.83	17.24	17.16	17.44	17.28	9.28	10.79	22.33	22.64	22.51	21.94	22.87	22.71	1.37
NiO	0.00	0.00	0.00	0.00	0.00	0.03	0.00	0.05	0.00	0.00	0.02	0.00	0.00	0.00	0.02
MgO	11.93	11.94	11.58	12.41	11.72	12.73	15.99	14.49	16.97	17.07	17.78	17.25	17.27	17.34	0.10
CaO	10.35	10.51	10.76	10.37	10.56	10.17	11.77	11.78	2.27	1.48	1.40	2.27	1.43	1.45	1.27
Na_2O	1.22	1.27	1.40	1.33	1.30	1.19	2.13	1.94	0.43	0.33	0.20	0.35	0.26	0.21	2.09
K_2O	0.38	0.49	0.54	0.45	0.54	0.35	0.45	0.53	0.05	0.00	0.00	0.04	0.00	0.00	3.05
F	0.00	0.00	0.00	0.00	0.00	0.00	0.00	0.00	0.00	0.00	0.00	0.00	0.00	0.00	0.00
Cl	0.14	0.17	0.14	0.14	0.16	0.13	0.01	0.04	0.05	0.04	0.04	0.05	0.05	0.04	0.21
Init. tot	*97.51*	*97.96*	*98.08*	*98.33*	*98.02*	*97.58*	*97.21*	*98.25*	*98.10*	*97.47*	*97.81*	*98.10*	*98.43*	97.70	*93.96*
*FeO	12.03	10.71	12.83	11.55	12.00	11.23	3.81	6.05	20.17	21.24	21.18	20.05	22.00	21.51	
*Fe_2O_3	6.12	7.91	4.90	6.24	6.05	6.72	6.07	5.26	2.41	1.56	1.48	2.10	0.97	1.34	
*H_2O^+	2.00	1.99	1.99	2.00	1.99	2.01	2.08	2.06	2.04	2.04	2.05	2.04	2.04	2.04	
Tot.	*100.13*	*100.74*	*100.56*	*100.95*	*100.62*	*100.27*	*99.90*	*100.84*	*100.38*	*99.67*	*100.01*	*100.35*	*100.56*	*99.87*	
Si	6.805	6.592	6.636	6.743	6.674	6.801	6.146	6.150	7.622	7.701	7.761	7.641	7.769	7.748	
Al	1.195	1.408	1.364	1.257	1.326	1.199	1.854	1.850	0.378	0.299	0.239	0.359	0.231	0.252	
Sr	0.000	0.000	0.000	0.000	0.000	0.000	0.000	0.000	0.000	0.000	0.000	0.000	0.000	0.000	
Fe	0.000	0.000	0.000	0.000	0.000	0.000	0.000	0.000	0.000	0.000	0.000	0.000	0.000	0.000	
Mg	*8.000*	*8.000*	*8.000*	*8.000*	*8.000*	*8.000*	*8.000*	*8.000*	*8.000*	*8.000*	*8.000*	*8.000*	*8.000*	*8.000*	
Ti	0.095	0.125	0.205	0.134	0.153	0.114	0.189	0.179	0.036	0.029	0.023	0.037	0.023	0.028	
Al	0.252	0.188	0.228	0.216	0.234	0.160	0.326	0.493	0.034	0.067	0.032	0.050	0.084	0.047	
Cr	0.002	0.001	0.001	0.001	0.005	0.000	0.014	0.000	0.000	0.000	0.000	0.000	0.000	0.002	
Fe^{3+}	0.677	0.873	0.544	0.685	0.669	0.742	0.657	0.568	0.263	0.173	0.161	0.228	0.106	0.147	
Ni	0.000	0.000	0.000	0.000	0.000	0.003	0.000	0.006	0.000	0.000	0.002	0.000	0.000	0.000	
Fe^{2+}	1.355	1.202	1.480	1.268	1.374	1.199	0.385	0.660	0.984	1.002	0.926	0.949	1.051	0.999	
Mg	2.619	2.611	2.541	2.697	2.566	2.783	3.429	3.094	3.683	3.728	3.858	3.736	3.735	3.777	
C subtot	*5.000*	*5.000*	*4.999*	*5.001*	*5.001*	*5.001*	*5.000*	*5.000*	*5.000*	*4.999*	*5.000*	*5.000*	*4.999*	*5.000*	
Mn^{2+}	0.068	0.060	0.044	0.055	0.059	0.056	0.013	0.025	0.113	0.121	0.100	0.109	0.120	0.114	
Fe^{2+}	0.127	0.111	0.099	0.140	0.100	0.179	0.073	0.065	1.472	1.599	1.654	1.488	1.618	1.629	
Ca	1.633	1.651	1.697	1.620	1.662	1.597	1.814	1.808	0.354	0.233	0.218	0.354	0.222	0.227	
Na	0.172	0.178	0.161	0.185	0.179	0.167	0.099	0.102	0.060	0.047	0.028	0.049	0.040	0.029	
B subtot	*2.000*	*2.000*	*2.001*	*2.000*	*2.000*	*1.999*	*1.999*	*2.000*	*1.999*	*2.000*	*2.000*	*2.000*	*2.000*	*1.999*	
Na	0.176	0.182	0.238	0.190	0.192	0.171	0.496	0.438	0.060	0.047	0.028	0.049	0.035	0.029	
K	0.071	0.091	0.102	0.083	0.101	0.066	0.082	0.096	0.009	0.000	0.000	0.007	0.000	0.001	
A subtot	*0.247*	*0.273*	*0.340*	*0.273*	*0.293*	*0.237*	*0.578*	*0.534*	*0.069*	*0.047*	*0.028*	*0.056*	*0.035*	*0.030*	
O	22.000	22.000	22.000	22.000	22.000	22.000	22.000	22.000	22.000	22.000	22.000	22.000	22.000	22.000	
OH	1.965	1.958	1.966	1.964	1.960	1.969	1.997	1.990	1.987	1.989	1.990	1.987	1.989	1.989	
F	0.000	0.000	0.000	0.000	0.000	0.000	0.000	0.000	0.000	0.000	0.000	0.000	0.000	0.000	
Cl	0.035	0.042	0.034	0.036	0.040	0.031	0.003	0.010	0.013	0.011	0.010	0.013	0.011	0.011	
W subtot	*2.000*	*2.000*	*2.000*	*2.000*	*2.000*	*2.000*	*2.000*	*2.000*	*2.000*	*2.000*	*2.000*	*2.000*	*2.000*	*2.000*	
Cat Sum	15.247	15.273	15.34	15.274	15.294	15.237	15.577	15.534	15.068	15.046	15.028	15.056	15.034	15.029	
X_{Fe}									0.396	0.405	0.396	0.388	0.405	0.403	

Bt–Amp andesite conglomerate (Fig. 4). Based on this fact, the provenance of cummingtonite from volcanic rocks of rhyolitic composition can be excluded. Red or rusty colouration of volcanic lithoclasts of the second type is caused by replacement of volcanic glass by Fe^{3+}-rich clay minerals of the smectite group (Table 1). They are a typical alteration product of volcanic glass, where the source of Fe and Mg can be found in the decay of mafic minerals (e.g., Treiman et al. 2014).

Similar mineral and textural composition of the well lithified volcanic rock of the first type (purple, greenish-grey) relative to underlying volcanic conglomerate indicated their older age. Reddish-brown coloured, cummingtonite-bearing volcanic lithoclasts (type 2) are not present in underlying sediments and this points to their younger age. Rusty colouration is typical for rapid cooling of volcanic clasts in oxidizing conditions. If exposed to water, the degree of alteration of some lithoclasts will cause their disintegration and washout. This excludes redeposition in a marine environment after their deposition and alteration. In addition, amphibole and pyroxene are unstable heavy minerals with rapid decay during weathering, transportation and burial depth (e.g., Morton 1984; Morton & Hallswort 1999; Andò et al. 2012). The presence of fresh amphibole and pyroxene in mineral grains, as well as inside the volcanic clasts, points to rapid sedimentation, short transport and low burial depth. Based on these facts, rusty coloured volcanic lithoclasts, fresh amphibole and pyroxene phenocrysts can be considered syn-depositional. As is mentioned earlier, the Bt–Amp andesite conglomerate (1346–1351 m and 1099–1104 m) corresponds to the Studenec Fm. (3rd caldera stage according to Konečný et al. 1998a; Konečný & Lexa 2001; Konečný et al. 2001). This is supported by similar chemical composition of Bt–Amp lithoclasts and andesites of the Studenec Fm. (Fig. 6). Therefore, cummingtonite-bearing

Table 4: The composition of selected pyroxene from heavy fraction of Zm-1 well (depth 1005–1010 and 1046–1051 m).

grain	1 core	1 rim	2	3
SiO_2	50.92	48.80	50.63	50.85
TiO_2	0.39	0.74	0.67	0.71
Al_2O_3	1.73	4.48	2.34	2.56
Cr_2O_3	0.02	0.37	0.02	0.03
FeO	7.72	1.89	9.10	7.87
Fe_2O_3	3.30	4.87	2.59	3.48
MgO	14.00	15.80	13.98	14.94
MnO	0.38	0.19	0.32	0.37
CaO	20.96	21.43	19.56	19.58
Na_2O	0.29	0.29	0.37	0.32
Total	*99.71*	*98.86*	*99.59*	*100.69*
Si	1.914	1.817	1.906	1.887
Al	0.077	0.183	0.094	0.112
Fe^{3+}	0.009	0.000	0.000	0.001
subtot T	2.000	2.000	2.000	2.000
Al	0.000	0.014	0.010	0.000
Fe^{3+}	0.093	0.137	0.073	0.097
Ti	0.011	0.021	0.019	0.020
Cr	0.001	0.011	0.001	0.001
Mg	0.784	0.818	0.785	0.826
Fe^{2+}	0.111	0.000	0.112	0.056
subtot M1	1.000	1.000	1.000	1.000
Mg^{2+}	0.000	0.059	0.000	0.000
Fe^{2+}	0.132	0.059	0.174	0.188
Mn	0.012	0.006	0.010	0.011
Ca	0.844	0.855	0.789	0.779
Na	0.021	0.021	0.027	0.023
subtot M2	1.010	1.001	1.001	1.002

volcanic lithoclasts should be connected with subsequent volcanic activity. The age range of the 4th evolutionary stage of the Štiavnica stratovolcano is 12.7 to 12.2 Ma (Chernyshev et al. 2013). This is consistent with biostratigraphic data from the studied samples (NN6 Zone, depth 1046–1051 m; Šarinová et al. 2018). The 4th post-caldera stage is represented by Obyce, Ladzany, Baďany, Biely Kameň, Drastvica, Priesil, Inovec fms. and by the Humenica, Sitno, Žiar, Jabloňový vrch, Breznica complexes (Konečný et al. 1998a). However, a lot of these formations and complexes are composed of pyroxene andesites. The Ladzany, Biely Kameň and Drastvica fms. are formed by Px–Bt–Amp dacites to andesites, but the Ladzany Fm. is only found in the southern parts of the stratovolcano (Konečný et al. 1998a,b). In addition, experimental works (Oba & Nicholls 1986; Geschwind & Rutherford 1992;

Table 5: The composition of amphiboles from Bt–Amp andesite to dacite conglomerate; *values were calculated according to Locock (2014).

depth	1099–1104 m			1346–1351 m							
species	magnesio-hastingsite to ferri-sadanagaite			magnesio-hastingsite						magnesio-ferri-hornblende	
grain	1	2	3	1	2	3	4 core	4 rim	5	6	7
SiO_2	42.29	42.38	41.87	41.92	42.33	41.95	43.27	43.80	42.92	44.63	46.50
TiO_2	2.52	2.34	2.36	2.06	2.36	2.06	2.44	2.37	2.44	1.61	1.13
Al_2O_3	13.18	13.59	13.14	12.04	13.19	13.57	11.18	12.25	13.18	9.10	7.67
Cr_2O_3	0.00	0.04	0.00	0.02	0.04	0.02	0.01	0.04	0.00	0.01	0.02
MnO	0.14	0.12	0.16	0.28	0.15	0.17	0.20	0.21	0.16	0.43	0.52
FeO	10.64	10.18	11.39	13.88	11.43	12.29	14.24	11.06	10.96	18.15	17.56
NiO	0.00	0.00	0.00	0.03	0.00	0.02	0.04	0.02	0.00	0.01	0.01
MgO	15.39	15.17	14.74	12.98	14.28	14.08	13.15	15.51	15.07	11.74	12.30
CaO	11.32	11.36	11.12	11.06	11.65	11.61	11.58	11.63	11.89	10.95	10.55
Na_2O	2.33	2.17	2.08	3.28	2.23	2.05	2.00	2.10	2.06	1.46	1.79
K_2O	0.47	0.54	0.63	0.55	0.52	0.59	0.54	0.54	0.58	0.61	0.36
F	0.00	0.00	0.00	0.93	0.00	0.00	0.00	0.00	0.00	0.00	0.00
Cl	0.03	0.02	0.03	0.08	0.03	0.03	0.05	0.04	0.03	0.16	0.13
Init. Tot	*98.30*	*97.93*	*97.51*	*98.70*	*98.21*	*98.44*	*98.69*	*99.56*	*99.29*	*98.81*	*98.52*
*FeO	5.01	5.24	5.36	10.85	7.27	6.43	10.09	5.78	5.98	11.92	12.68
*Fe_2O_3	6.26	5.50	6.69	3.36	4.63	6.51	4.60	5.88	5.54	6.92	5.43
*H_2O^+	2.07	2.07	2.06	1.56	2.05	2.05	2.02	2.06	2.06	1.98	1.99
Total	*101.00*	*100.55*	*100.24*	*100.60*	*100.72*	*101.15*	*101.17*	*102.21*	*101.90*	*101.48*	*101.05*
Si	6.054	6.081	6.056	6.176	6.113	6.042	6.294	6.200	6.102	6.539	6.809
Al	1.946	1.919	1.944	1.824	1.887	1.958	1.706	1.800	1.898	1.461	1.191
T subtot	*8.000*	*8.000*	*8.000*	*8.000*	*8.000*	*8.000*	*8.000*	*8.000*	*8.000*	*8.000*	*8.000*
Ti	0.271	0.253	0.257	0.228	0.256	0.223	0.266	0.252	0.261	0.177	0.124
Al	0.278	0.379	0.297	0.267	0.358	0.345	0.210	0.243	0.310	0.110	0.133
Cr	0.000	0.004	0.000	0.002	0.004	0.003	0.001	0.005	0.000	0.002	0.003
Fe^{3+}	0.673	0.594	0.729	0.373	0.502	0.706	0.505	0.626	0.593	0.762	0.597
Ni	0.000	0.000	0.001	0.003	0.001	0.002	0.005	0.003	0.000	0.001	0.001
Fe^{2+}	0.494	0.524	0.539	1.276	0.804	0.698	1.160	0.597	0.642	1.383	1.457
Mg	3.283	3.245	3.178	2.850	3.075	3.024	2.852	3.274	3.194	2.565	2.685
C subtot	*4.999*	*4.999*	*5.001*	*4.999*	*5.000*	*5.001*	*4.999*	*5.000*	*5.000*	*5.000*	*5.000*
Mn^{2+}	0.017	0.015	0.020	0.035	0.018	0.021	0.024	0.025	0.020	0.053	0.065
Fe^{2+}	0.107	0.104	0.110	0.061	0.075	0.076	0.067	0.086	0.069	0.079	0.097
Ca	1.737	1.747	1.724	1.746	1.803	1.792	1.805	1.763	1.811	1.719	1.656
Na	0.140	0.134	0.147	0.158	0.105	0.111	0.104	0.126	0.101	0.149	0.182
B subtot	*2.001*	*2.000*	*2.001*	*2.000*	*2.001*	*2.000*	*2.000*	*2.000*	*2.001*	*2.000*	*2.000*
Na	0.506	0.471	0.437	0.780	0.519	0.462	0.460	0.451	0.468	0.267	0.325
K	0.086	0.099	0.116	0.103	0.096	0.109	0.101	0.097	0.105	0.114	0.067
A subtot	*0.592*	*0.570*	*0.553*	*0.883*	*0.615*	*0.571*	*0.561*	*0.548*	*0.573*	*0.381*	*0.392*
O	22.000	22.000	22.000	22.000	22.000	22.000	22.000	22.000	22.000	22.000	22.000
OH	1.993	1.996	1.992	1.546	1.992	1.992	1.988	1.990	1.992	1.960	1.967
F	0.000	0.000	0.000	0.434	0.000	0.000	0.000	0.000	0.000	0.000	0.000
Cl	0.007	0.004	0.008	0.019	0.008	0.008	0.012	0.010	0.008	0.040	0.033
W subtot	2.000	2.000	2.000	*1.999*	*2.000*	*2.000*	*2.000*	*2.000*	*2.000*	*2.000*	*2.000*
Cat sum	15.592	15.569	15.555	15.882	15.616	15.572	15.560	15.548	15.574	15.381	15.392

Table 6: Whole rock chemical composition of lithoclasts from Bt–Amp andesite conglomerates; ZM-1/18: depth 1346–1351 m; ZM-1/13: 1099–1104 m; n.d. — under detection limit.

sample	SiO_2 wt. %	Al_2O_3 wt. %	Fe_2O_3 wt. %	MgO wt. %	CaO wt. %	Na_2O wt. %	K_2O wt. %	TiO_2 wt. %	P_2O_5 wt. %	MnO wt. %	Cr_2O_3 wt. %	LOI %	sum %	Ctot %	Zr ppm	Nb ppm	Rb ppm	Sr ppm	Ta ppm
ZM-1/18	59.27	17.21	6.17	2.42	5.81	3.13	2.34	0.64	0.18	0.14	n.d.	2.5	99.81	0.17	132.4	14.4	106.8	105.7	1.4
ZM-1/13	58.28	17.33	6.94	2.73	5.75	3.27	2.32	0.65	0.19	0.09	0.002	2.3	99.85	0.21	109.9	13.1	76.5	346.8	0.8
sample	**Th ppm**	**U ppm**	**Ga ppm**	**Hf ppm**	**Y ppm**	**La ppm**	**Ce ppm**	**Pr ppm**	**Nd ppm**	**Sm ppm**	**Eu ppm**	**Gd ppm**	**Tb ppm**	**Dy ppm**	**Ho ppm**	**Er ppm**	**Tm ppm**	**Yb ppm**	**Lu ppm**
ZM-1/18	18.2	4.1	14.8	4.3	17.7	34.3	56.5	6.43	20.9	3.76	0.70	3.45	0.54	3.15	0.64	1.97	0.31	2.18	0.33
ZM-1/13	9.8	2.4	15.0	2.9	16.8	28.1	51.9	5.52	19.3	3.53	0.96	3.34	0.53	3.10	0.61	1.91	0.28	1.82	0.29

Nicholls et al. 1992; Evans & Ghiorso 1995) suggest that the full temperature range of cummingtonite (volcanic & metamorphic) is ca. 400–800 °C. High water-pressure storage is also necessary. The presence of cummingtonite in volcanic rocks is connected with temperature between 700–840 °C, P < 300 MPa, conditions close to water saturation and shallow magma chamber (Geschwind & Rutherford 1992; Smith et al. 2005). High water saturation is connected with explosive volcanism. From this point of view, Drastvica Fm. is the most likely source of cummingtonite-bearing lithoclasts. This formation consists of products of amphibole-rich explosive volcanism (ignimbrite and pumice tuff of Px–Amp andesite+Bt; Konečný et al. 1998a) and overlies the Studenec Fm. Both formations are in close proximity to the ZM-1 well (Konečný et al. 1998b). The presented results from the studied samples are consistent with these data. On the other hand, the Priesil Fm. is composed of Amp–Px andesites with variable colouration. In this case, the Px versus Amp ratio is in favour of Px (Konečný et al. 1998a). But this is not consistent with results from the studied samples, where amphibole dominated. However, this hypothesis must be confirmed in the future. The fact, that cummingtonite-bearing volcanic rocks have not yet been described in the Štiavnica volcanic field may also be explained by their complete erosion.

The depositional mechanism of the studied samples can be deduced from textural features and petrographical composition, but the core samples do not allow a clear interpretation. Poor sorting, together with variable roundness of lithoclasts, presence of calcareous fossils, framboidal pyrite, synsedimentary folds, slumps and erosional surfaces indicated deposition by sediment gravity flows in a marine environment. Crystal shape of mineral grains and presence of unstable heavy minerals also indicates short transport. The epiclastic origin can be deduced from mixing of non-volcanic and volcanic grains of various ages, from roundness of clasts, by presence of mud intraclasts and fossils. Welding and other thermal effects typical for hot pyroclastic flows are not observed. Well sorted sandstones with indistinct ripples are rare and present only on small portions of the well core. Their deposition can therefore be explained by traction as well as by turbiditic transport. Either way, their epiclastic origin is indisputable and so transport by pyroclastic flows can be excluded. In this point of view, a delta front environment (delta slope morphology) influenced by volcanic activity is assumed. Sizes of friable, rusty coloured volcanic fragments (up to 1 cm in diameter) and epiclastic origin of the studied samples may point to deposition in the middle or distal zone of the volcanic centre. Non-volcanic admixture is similar to that in underlying sediments and points to their recycling.

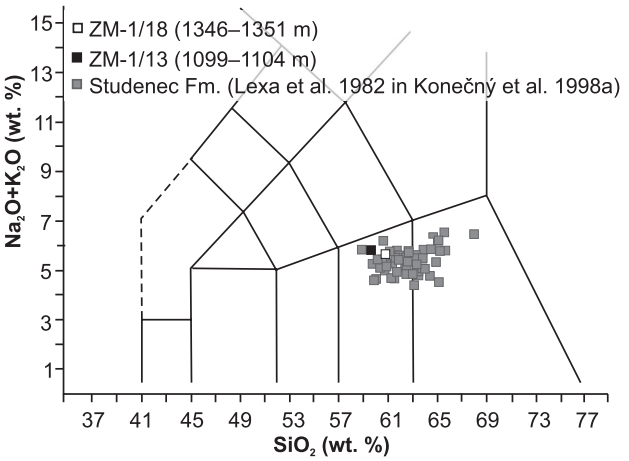

Fig. 6. Comparison of chemical compositions of Bt-Amp andesite lithoclasts (depth 1346–1351 m and 1099–1104 m, ZM-1 well) with data from the Studenec Fm. (Lexa et al. 1997 in Konečný et al. 1998a).

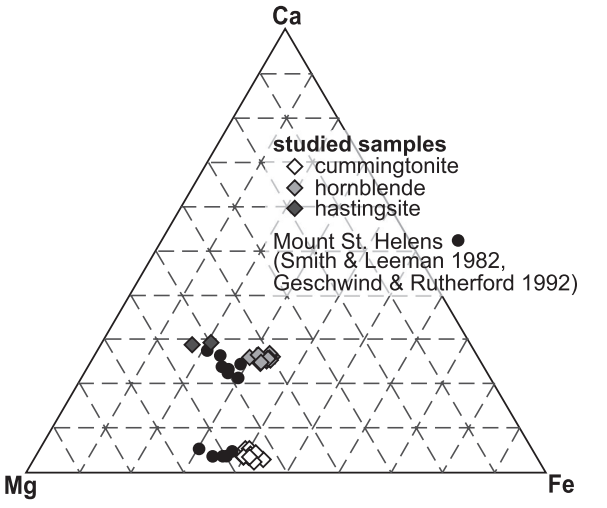

Fig. 7. Ca–Mg–Fe diagram to illustrate the relationship of amphibole (Hbl and Cum) from the studied samples (1005–1051 m). For comparison, the composition of amphibole from Yn tephra of Mount St. Helens is displayed (data from Smith & Leeman 1982; Geschwind & Rutherford 1992).

On the other hand, presence of different, Pannonian (Tortonian) fossil assemblages in samples from the depth of 1005–1010 m (Šarinová et al. 2018) indicate reworking of sediments from the depth of 1046–1051 m. This is confirmed by increase of roundness and admixture of non-volcanic grains. In this depth interval, strongly altered volcanic lithoclasts of the second type (which produce secondary pore space) are not present. The redeposition can be linked to sea level change or to the wide rifting of the Danube Basin in the Sarmatian–Panonian (Serravallian–Tortonian) stage (e.g., Kováč et al. 2017).

Conclusion

The observed mineral association: plagioclase, cummingtonite, hornblende and pyroxene, is typical for cummingtonite-bearing volcanic rocks for localities all around the world. The presence of cummingtonite phenocrysts in volcanic lithoclasts clearly documents its volcanic origin. Based on the succession of volcanic rocks and biostratigraphic ranking of sediments (Šarinová et al. 2018), the cummingtonite-bearing lithoclasts are derived from formations of the 4th evolutionary stage of the Štiavnica stratovolcano (Konečný et al. 1998a,b; Chernyshev et al. 2013). The Drastvica Fm. corresponds well to the conditions for production of cummingtonite-bearing volcanic rocks, as well as to the observed mineral association and geological structure of the studied area. Finding of parental rocks of such volcanic lithoclasts will be important for future study of the Štiavnica stratovolcano evolution, likewise for provenance analysis and indirect dating of sediments.

Acknowlegements: This research was supported by the Slovak research and development agency under the contracts No. APVV-0099-11, APVV-15-0575 & APVV-16-0121. Our special thanks go to Nafta Petroleum Company management for allowing access to their well core repository. We express our gratitude to the editor and to the reviewers for their insightful comments which improved the manuscript.

References

Andò S., Garzanti E., Padoan M. & Limonta M. 2012: Corrosion of heavy minerals during weathering and diagenesis: A catalog for optical analysis. *Sediment. Geol.* 280, 165–178.

d'Arco Ph., Maury R.C. & Westercamp D. 1981: Geothermometry and geobarometry of a cummingtone-bearing dacite from Martinique, Lesser Antilles. *Contrib. Mineral. Petrol*. 77, 177–184.

Biela A. 1978: Deep wells of the inner Western Carpathians I. *Regionálna geológia Záp. Karpát* 10, *GÚDŠ*, 1–224 (in Slovak).

Dropp G.T.R. 1987: A general evaluation for estimating Fe^{3+} concentrations in ferromagnesian silicates and oxides from microprobe analyses, using stoichiometric criteria. *Mineral. Mag.* 51, 431–435.

Evans B.W. & Ghiorso M.S. 1995: Thermodynamics and petrology of cummingtonite. *Am. Mineral.* 80, 649–663.

Ewart A. & Green D.C. 1971: Voluminous Low Temperature Rhyolitic Magmas in New Zeland. *Contrib. Mineral. Petrol.* 33, 128–144.

Ewart A., Hildreth W. & Carmichael I.S.E. 1975: Quaternary Acid Magma in New Zealand *Contrib. Mineral. Petrol.* 51, 1–27.

Faryad S.W. & Zábranský F. 1996: Newly found rock-forming minerals in the eastern part of the Slovak Ore Mountains, Western Carpathians, Slovakia. *Acta Montanistica Slovaca* 1, 2, 131–138.

Hraško Ľ., Antalík M., Bačo P., Bačová Z., Bezák V., Boorová D., Bóna J., Buček S., Čech P., Demko R., Derco J., Elečko M., Filo I., Ferenc Š., Fordinál K., Gazdačko Ľ., Gaži P., Gluch A., Gross P., Harčová E., Havrila M., Havrila J., Kášer Š., Kobulský J., Kohút M., Kollárová V., Konečný P., Konečný V., Kováčik M., Kováčik M., Kováčiková M., Kováčová M., Kráľ J., Kronome B., Kubeš P., Kučera M., Laurinc D., Madarás J., Maglay J., Németh Z., Olšavský M., Pécskay Z., Pešková I., Potfaj M., Premuka S., Pristaš J., Radvanec M., Siráňová Z., Šimon L., Šimonová B., Vaněková H., Vlachovič J., Zlinská A. & Žecová K. 2014: Results of the geological task "Update of the geological setting of problematic areas in the Slovak Republic at a scale 1 : 50,000". *Geologické práce, Správy* 124, 7–66 (in Slovak).

Hawthorne F.C., Oberti R.,Harlow G.E., Maresch W.V., Martin R.F., Schumacher J.C. & Welch M.D. 2012: IMA report, nomenclature of the amphibole supergroup. *Am. Mineral.* 97, 2031–2048.

Geschwind C-H. & Rutherford M.J. 1992: Cummingtonite and the evolution of the Mount St Helens (Washington) magma system: An experimental study. *Geology* 20, 1011–1014.

Chernyshev I.V., Konečný V., Lexa J., Kovalenker V. ., Jeleň S., Lebedev V.A. & Goltsman Y.V. 2013: K–Ar and Rb–Sr geochronology and evolution of the Štiavnica Stratovolcano (Central Slovakia). *Geol. Carpath.* 64, 4, 327–351.

Janák M., Plašienka D. & Petrík I., 2001: Excursion to the Tatra Mountains, Central Western Carpathians: Tectonometamorphic Records of Variscan and Alpine Orogeny. *GeoLines* 13, 141–148.

Káčer Š. (Ed.), Polák M., Bezák V., Hók J., Teťák F., Konečný V., Kučera M., Žec B., Elečko M., Hraško Ľ., Kováčik M., Pristaš J., Káčer Š., Antalík M., Lexa J., Zvara I., Fritzman R., Vlachovič J., Bystrická G., Brodianska M., Potfaj M., Madarás J., Nagy A., Maglay J., Ivanička J., Gross P., Rakús M., Vozárová A., Buček S., Boorová D., Šimon L. & Mello J. 2013: Slovak Republic — digital geological map in scale of 1:50,000 and 1:500,000. *Geol. Inst. of Dionýz Štúr*, http://apl.geology.sk/gm50js.

Kollárová V. 2010: Petrography and petrology of rhyolite rocks from the Poľana stratovolcano. In: Demko R. (Ed). et al.: Maps of paleovolcanic reconstruction of rhyolite volcanic of Slovakia and analyse of magmatic and hydrothermal proceses. Final report of the geological task 15 06. *Open file report, Geofond*, Bratislava, 455–510 (in Slovak).

Konečný V. (Ed), Lexa J., Halouzka R., Hók J., Vozár J., Dublan L., Nagy A., Šimon L., Havrila M., Ivanička J., Hojstovičová V., Miháliková A., Vozárová A., Konečný P., Kováčikova M., Filo M., Marcin D., Klukanová A., Liščák P. & Žáková E. 1998a: Explanatory notes for the geological map of Štiavnické vrchy Mts. and Pohronský Inovec Mts. (Štiavnica stratovolcano). *Geol. Inst. of Dionýz Štúr*, Bratislava, 1–473 (in Slovak).

Konečný V. (Ed), Lexa J., Halouzka R., Dublan L., Šimon L., Stolár M., Nagy A., Polák M., Vozár J., Havrila M. & Pristaš J. 1998b: Geological map of the region Štiavnické vrchy Mts. And Pohronský Inovec Mts. 1: 50,000. *Geol. Inst. of Dionýz Štúr*, Bratislava.

Konečný V., Lexa J., Šimon L. & Dublan L. 2001: The neogene volcanism in central Slovakia. *Mineralia Slovaca* 33, 159–178 (in Slovak).

Konečný V. & Lexa J. 2001: Structure and evolution of the Štiavnica stratovolcano. *Mineralia Slovaca* 33, 179–196 (in Slovak).

Kováč M., Hudáčková N., Halásová E., Kováčová M., Holcová K., Oszczypko-Clowes M., Báldi K., Less G., Nagymarosy A., Ruman A., Klučiar T. & Jamrich M. 2017: The Central Paratethys palaeoceanography: a water circulation model based on microfossil proxies, climate, and changes of depositional environment. *Acta Geologica Slovaca* 9, 2, 75–114.

Locock A.J. 2014: An Excel spreadsheet to classify chemical analyses of amphiboles following the IMA 2012 recommendations. *Computers & Geosciences* 62, 1–11.

Lowe D.J. & Hunt J.B. 2001: A summary of terminology used in tephra-related studies. In: Juvigné E.T. & Raynal J-P. (Eds.): Tephras: Chronology, Archeology. *CDERAD éditeur*, Goudet. *Les Dossiers de l´Archéo-Logis* 1, 17–22.

Matsu'ura T., Furusawa A. & Yanagida M. 2012: Detection and correlation of widespread cryptotephras in middle Pleistocene loess in NE Japan using cummingtonite geochemistry, *J. Asian Earth Sci.* 60, 49–67.

Morton A.C. 1984: Stability of detrital heavy minerals in tertiary sandstones from the North sea basin. *Clay Miner.* 19, 287–308.

Morton A.C. & Hallswort C.R. 1999: Processes controlling the composition of heavy mineral assemblages in sandstones. *Sediment. Geol.* 124, 3–99.

Mullineaux D.R. 1986: Summary of pre-1980 tephra-fall deposits erupted from Mount St. Helens, Washington State, USA. *Bull. Volcanol.* 48, 17–26.

Nicholls I.A., Oba T. & Conrad W.K. 1992: The nature of primary rhyolitic magmas involved in crustal evolution: Evidence from an experimental study of cummingtonite-bearing rhyolites, Taupo Volcanic Zone, New Zealand. *Geochim. Cosmochim. Acta* 56, 3, 955–962.

Oba T. & Nicholls I.A. 1986: Experimental Study of cummingtonite and Ca–Na amphibole relations in the system Cum–Act–Pl–Qz–H_2O. *Am. Mineral.* 71, 1354–1365.

Ozdínová S. 2012: Redepositions of the Paleogene calcareous nannofossils in the Neogene sediments around the northern margin of the Danube Basin: The data source about uplift and erosion of the substrates. *Mineralia Slovaca* 44, 257–266 (in Slovak).

Pal T., Mitra S.K., Sengupta S., Katari A., Bandopadhyay P.C. & Bhattacharya A.K. 2007: Dacite-andesites of Narcondam volcano in the Andaman Sea — An imprint of magma mixing in the inner arc of the Andaman-Java subduction system. *J. Volcanol. Geotherm. Res.* 168, 93–113.

Pedersen A.K. & Hald N. 1982: A cummingtonite-porphyritic dacite with amphibole-rich xenoliths from the tertiary central volcano at Króksfjördur, NW Iceland. *Lithos* 15, 2, 137–159.

Smith D.R. & Leeman W.P. 1982: Mineralogy and phase chemistry of Mount St. Helens tephra sets W and Y as key to their identification. *Quaternary Res.* 17, 211–227.

Smith V.C., Shane P. & Nairn I.A. 2005: Trend in rhyolite geochemistry, mineralogy, and magma storage during the last 50 kyr at Okataina and Taupo volcanic centers, Taupo Volcanic Zone, New Zealand. *J. Volcanol. Geotherm. Res.* 148, 372–406.

Šarinová K., Rybár S., Halásová E., Hudáčková N., Jamrich M., Kováčová M. & Šujan M. 2018: Integrated biostratigraphical, sedimentological and provenance analyses with implications for lithostratigraphic ranking: the Miocene Komjatice depression of the Danube Basin. *Geol. Carpath.* 69, 382–409.

Treiman A.H., Morris R.V., Agresti D.G., Graff T.G., Achilles Ch.N., Rampe E.B., Bristow T.F., Ming D.W., Blake D.F., Vaniman D.T., Bish D.L., Chipera S.J., Morrison S.M. & Downs R. 2014: Ferrian saponite fron the Santa Monica Mountains (California, U.S.A., Earth): Characterization as an analog for clay minerals on Mars with application to Yellowknife Bay in Gale Crater. *Am. Mineral.* 99, 2234–2250.

Whitney D.L. & Evans B.W. 2010: Abbreviattions for names of rock-forming minerals. *Am. Mineral.* 95, 185–187.